Magnetic Backscatter for In-body Communication and Localization

Bill Tao, Emerson Sie, Jayanth Shenoy, Deepak Vasisht
University of Illinois Urbana-Champaign

ABSTRACT

Implantable and edible medical devices promise to provide continuous, directed, and comfortable healthcare treatments. Communicating with such devices and localizing them is a fundamental, but challenging, mobile networking problem. Recent work has focused on leveraging near field magnetism-based systems to avoid the challenges of attenuation, refraction, and reflection experienced by radio waves. However, these systems suffer from limited range, and require fingerprinting-based localization techniques. We present InnerCompass, a magnetic backscatter system for in-body communication and localization. InnerCompass relies on new magnetism-native design insights that enhance the range of these devices. We design the first analytical model for magnetic-field-based localization, that generalizes across different scenarios. We've implemented InnerCompass and evaluated it in porcine tissue. Our results show that InnerCompass can communicate at 5 Kbps at a distance of 25 cm, and localize with an accuracy of 5 mm.

CCS CONCEPTS

• **Hardware → Bio-embedded electronics**; • **Networks → Wireless personal area networks**; • **Human-centered computing → Mobile computing**.

KEYWORDS

In-body Computing, Magnetism, Localization

ACM Reference Format:
Bill Tao, Emerson Sie, Jayanth Shenoy, Deepak Vasisht. 2023. Magnetic Backscatter for In-body Communication and Localization. In *The 29th Annual International Conference on Mobile Computing and Networking (ACM MobiCom '23), October 2–6, 2023, Madrid, Spain.* ACM, New York, NY, USA, 15 pages. https://doi.org/10.1145/3570361.3613301

ACM MobiCom '23, October 2–6, 2023, Madrid, Spain

ACM ISBN 978-1-4503-9990-6/23/10…$15.00
https://doi.org/10.1145/3570361.3613301

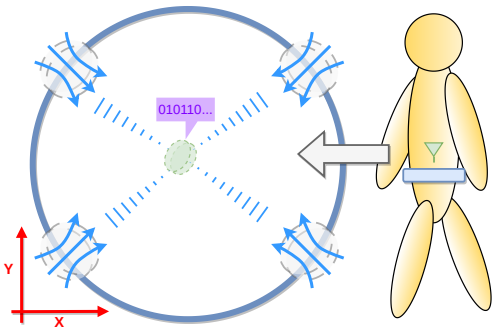

Figure 1: Overall structure of InnerCompass. We use multiple coils from different directions to localize and communicate with a tag inside the patient's body.

1 INTRODUCTION

In-body devices promise to transform modern medicine. These devices can be used for capsule endoscopy [6, 14], cancer radiation therapy [12, 18, 24], targeted drug delivery [15], and robot-driven abdominal insulin delivery [13, 37, 39]. As applications for such devices grow, there is wide interest in identifying optimal designs to communicate with such devices and to locate such devices inside the body. Traditional forms of communication such as Wi-Fi are too power-hungry for small in-body devices. Similarly, traditional forms of positioning such as X-rays, MRIs, and Ultrasound are either too cumbersome, expensive, or harmful to humans.

In general, any communication and localization techniques for such devices must meet the following constraints:

- **Size:** These devices must be small in size (centimeter-scale), so that they can be swallowed or implanted easily. Therefore, in-body communication systems cannot rely on large antennas.
- **Safety:** They should be safe for prolonged human use (unlike X-rays, for example).
- **Low Power:** In-body devices cannot carry large batteries due to their small size. So, they must operate with low power. In addition, high power use in-body might violate safety considerations.
- **Generalizable:** The techniques should generalize across humans with different body shapes and compositions.

- **Precise:** The location accuracy needs to be centimeter scale for applications like wireless endoscopy capsules [27] and mm-scale for cancer radiation therapy markers [12].

Much of past work has focused on Radio Frequency (RF) based low power communication solutions [1, 22]. However, RF-based solutions have several major shortcomings. First, the human body is inherently a challenging medium for radio waves due to its high water content. A large fraction of the signal is reflected at the human-air interface (skin) [40]. Once inside the human body, wireless signals experience exponential attenuation as they travel through muscle and fat. This problem is further exacerbated for localization applications because of refraction at every interface boundary (skin-fat, fat-muscle, muscle-air, skin-air, etc.). The signal deviates from its path at every interface and experiences different propagation speeds in each tissue type. Therefore, past work (e.g., [8, 40]) has come up with simplified human body models. Such approaches suffer in localization accuracy (a few centimeters of localization error) and tend to not-generalize across different body types and shapes.

Due to these challenges, recent work [30, 34, 35, 46, 48] has moved to magnetic communication and localization. magnetic fields do not interact with the human body, i.e., the human body is transparent to magnetic signals. Magnetic signals are also absorbed less by the human body and are safer as compared to RF signals. These systems rely on magnetic coupling between an external reader and an in-body coil. Due to their low frequencies, magnetic systems operate in near-field and can rely on signal strength for localization. In general, they measure the signal strength for different device locations at calibration time. They use this data to either do a nearest neighbor search (fingerprinting) or train a Machine Learning model (typically, a neural network). Although these approaches are precise, they require a lot of calibration effort during setup and are hard to generalize, especially if the relative locations of out-of-body coils vary due to body shape, breathing, or other variations.

We present InnerCompass, a magnetic backscatter-based localization and communication system for in-body devices that does not require any fingerprinting or model training. InnerCompass uses small tags and small out-of-body coils. It uses low-power magnetic backscatter for both communication and localization. It causes 100 dB less radiation exposure than is recommended as safe by the FCC. Due to the small size of the out-of-body coils, it can fit into wearables like smart belts or smart vests. Finally, it is generalizable – can work with different body shapes and across varying locations.

The key insight behind InnerCompass is – due to the minimal interaction between body tissues and magnetic fields, we do not need to create measurement-driven models for in-body localization. We can instead rely on analytical models created using simulations. Surprisingly, we show that it is easy to adapt the model from simulation to real-world, without requiring extensive calibration or real-world data collection. This allows us to analytically change our model for different body shapes or different deployment behaviors. To the best of our knowledge, we are the first to create such analytical models for magnetic localization. We are inspired by RF-based localization systems, where analytical far-field models like phased arrays have become the de facto standard for localization (having moved away from finger-printing-based localization). In building InnerCompass, we hope to engineer a similar shift in paradigm.

At a high level, InnerCompass uses a set of transmit-receive coils outside the body to magnetically couple with a small in-body tag. The tag can modulate the magnetic field to communicate data. As the location of the tag changes, the coupling coefficient changes inducing a variation in the signal strength of the signal received at receiver coils outside the body. In our design, we make the following interesting design decisions:

First, we note that magnetic localization systems require multiple RSSI (Received Signal Strength Indicator) measurements to perform a multi-dimensional localization. Prior work [34, 35] places multiple readers, i.e. a pair of transmit and receive coils, near the in-body device to get precise location. However, they treat each reader separately, thereby requiring N pairs of transmit-receive coils for N measurements. In contrast, we enabled all receivers to simultaneously receive from all transmitters, similar to the MIMO scheme, by letting the transmitting frequencies for each transmitter coil be slightly different from other transmitters. This enables us to obtain N^2 measured RSSIs from N pairs of coils. As a result, InnerCompass is able to obtain mm-level accuracy with only two sets of Tx and Rx coils, while state-of-the-art systems like [34] require six.

Second, different from traditional RF and magnetic communication systems, InnerCompass uses a customized transmit chain featuring a low impedance power amplifier and a series LC circuit coil. This design aims to increase the operating range of the system, so that it can communicate and localize devices deep inside human tissue, which requires increasing the signal strength transmitted by the reader. We observed that unlike traditional far-field communication devices, near field signal strength relies solely on the coil's current and not the power delivered to it. This lead us to a low impedance coil design, which increases the coil's current and the magnetic field generated.

We implemented a prototype of InnerCompass using off-the-shelf function generator, amplifiers, filters, ICs and a

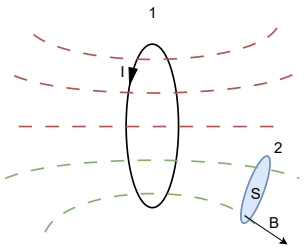

Figure 2: Two coils in proximity have inductive coupling. Coil 1 has a current I and generates a magnetic field. The part of the field that passes through coil 2 are marked in green.

2-layer printed circuit board (PCB). We tested the performance of InnerCompass in a lab and an office, using pork ribs as mock human tissue. Our results show that InnerCompass is able to obtain mm level accuracy. InnerCompass requires only one-time calibration *at manufacture time* using a single data point. Furthermore, we tested InnerCompass's ability to communicate data between the in-body device and the external reader, and found that InnerCompass is able to achieve as high as 5kbps data rate over a 25cm distance.

In designing InnerCompass, we make the following contributions:

- We build the first end-to-end analytical model for the RSSI of inductive coupling backscattering communication based on the underlying physics.
- We propose a MIMO-inspired localization strategy using frequency multiplexing that increases the localization accuracy and decrease the number of antennas needed.
- We propose a new way of designing coils for communication in near field, which minimizes the impedance on both the reader coil and the amplifier connected to it and increases the received signal strength.
- We built a prototype system, InnerCompass, and tested its performance in the real world.

2 BACKGROUND – INDUCTIVE COUPLING

When two coils are placed in proximity, they exhibit "inductive coupling", where current change in one coil, $\frac{dI_1}{dt}$, will stimulate voltage V_2 in the other. As a result, the magnetic field generated by one coil also passes through the other coil, as shown in Figure 2. The stimulated voltage satisfies [9]

$$V_2 = M_{1,2}\frac{dI_1}{dt}$$

where $M_{1,2}$ is a constant called "mutual inductance" depending on how much magnetic flux coil 1 generates on coil 2. The mutual inductance indicates the amount of magnetic flux on coil 2 caused by coil 1, and satisfies [9]

$$M_{1,2} = \frac{\Phi_{1,2}}{I_1}$$

Where $\Phi_{1,2}$ is the magnetic flux in coil 2 caused by coil 1. The magnetic flux is defined as [9]

$$\Phi = \int \mathbf{B} \cdot d\mathbf{S}$$

When the relative position of 1 and 2 are different, the magnetic field generated by 1 at 2's position would be different. Therefore, $M_{1,2}$ depends on the relative position between 1 and 2. Generally, when coil 2 is further away, the magnetic flux of coil 2 will be lower and $M_{1,2}$ will be lower.

3 INNERCOMPASS SYSTEM DESIGN

InnerCompass is a magnetic-based localization system designed to localize in-body deep tissue implants. InnerCompass design uses magnetic signals for backscatter localization of the implant rather than higher frequency RF signals for several key reasons:

- **Permeability:** InnerCompass's magnetic signal can easily penetrate all kinds of media including human body tissue that would typically attenuate or block RF signals.
- **No multipath:** InnerCompass uses low frequency magnetic signal allowing for near-field operation. In the near field, magnetic field energy degrades at $O(d^{-6})$, much faster than $O(d^{-2})$ decay for far field RF operation. As a result, magnetic signals do not experience the multipath reflections which often cause errors in RF-based localization.
- **Safety:** InnerCompass's magnetic signal is safer to use in human bodies. Magnetic field is non-radiative and at low frequencies, has a minimal absorption by tissues.
- **High Precision:** Magnetic signal energy degrades at a much faster rate than RF signals. This is an advantage for magnetic localization systems as it yields higher sensitivity and higher precision for measuring distance.

However, the properties of magnetic signals in near-field describe above lead to some inherent challenges for both communication and localization. First, the signal attenuates rapidly, as $O(d^{-6})$, with distance. This limits the range of operation of such devices. This is evident in the small range of off-the-shelf NFC devices, e.g., card readers and smartphones. To operate in-body, we need to enhance the range of these devices. Second, near field magnetic field does not fit the analytical models designed for far field localization systems. For example, state-of-the-art RF-based localization systems [17, 34, 40, 43], both in-body and in-air, rely on phase-based analytical models of far-field radio signals. Therefore, state-of-the-art work using magnetic fields has relied on fingerprinting-based models.

In InnerCompass, we solve these challenges. We present a new transmitter design in Sec. 3.2 that leverages unique insights for magnetic systems. We build the first analytical model for magnetic near-field localization in Sec. 3.3. We also present an optimization of our model in Sec. 3.4 that reduces the number of reader coils required for in-body localization.

3.1 InnerCompass's Backscatter Communication

Backscatter communication is widely used especially in devices with a tight energy budget. A backscatter communication system generally consists of a reader and a tag. Compared to traditional wireless communication systems, the tag does not emit its own signal. Instead, the reader sends a signal to the tag, and the tag modulates and reflects the signal from the reader to communicate. Since the tag does not need to transmit, it can run on very low power.

In InnerCompass, we design a backscatter communication system using the magnetic coupling mechanism. Our reader comprises of two coils: one transmit (Tx) coil and a separate receive (Rx) coil. The in-body tag comprises of a small coil as well. As shown in Figure 3, the Tx coil, the Rx coil, and the tag coil are mutually coupled. This coupling can be seen to operate in following steps.

Step 1: The Tx coil generates a magnetic field, B_{Tx}. The Tx chain sends an alternating current, I_{Tx} at frequency f into the Tx coil, which generates an alternating magnetic field B_{Tx}.

Step 2: The magnetic field B_{Tx} induces a current in the tag. The magnetic field $\mathbf{B}_{Tx}$ will generate a magnetic flux $\Phi_{Tx,tag}$ on the tag. From the definition of M we know that $\Phi_{Tx,tag} = M_{Tx,tag} I_{Tx}$. $\mathbf{B}_{Tx}$ is also an alternating magnetic field which, according to Faraday's law [9], will stimulate a voltage in the tag

$$V_{tag} = \frac{d\Phi_{Tx,tag}}{dt} = -2\pi j f I_{Tx} M_{Tx,tag}$$

According to Ohm's law [9], This voltage drives a current in the tag $I_{tag} = \frac{V_{tag}}{Z_{tag}}$ where Z_{tag} is the impedance of the tag circuit. The tag current, I_{tag} generates magnetic field $\mathbf{B}_{tag}$.

Step 3: The tag magnetic field, $\mathbf{B}_{tag}$, induces a current in the Rx coil. Similar to the case between Tx and tag, $\mathbf{B}_{tag}$ stimulates a voltage in the Rx coil

$$V_{Rx} = -2\pi j f I_{tag} M_{Rx,tag}$$

The voltage in the Rx coil then goes through the rest of the Rx chain including filters and amplifiers, and is sampled at our software defined radio.

3.1.1 Dealing with Tx-Rx Crosstalk. Tx signal can be received by Rx coil directly too, which can cause self-interference within the reader[1]. To avoid this problem, the InnerCompass tag modulates the signal and reflects it back to the receiver. We perform this modulation by employ a voltage-controlled switch operated by a fixed-frequency clock signal at the tag operating at frequency Δf. Given that the original signal frequency is f as defined above, the reflected signal has harmonic frequencies on $f + k\Delta f, k \in \mathbf{Z}$. We consider the component with the highest amplitude, e.g. $f - \Delta f$, as the signal to measure. On this frequency, we have $I'_{tag} = \epsilon \frac{V_{tag}}{Z_{tag}}$ where ϵ is the relative gain on the sideband. Subsequently, the received signal is $V'_{Rx} = 2\pi j f I'_{tag} M_{tag,Rx}$

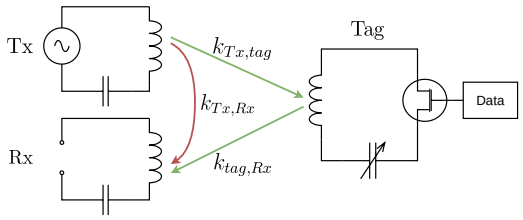

Figure 3: Magnetic coupling between the Tx, Rx, and tag coils. The self-interference is shown in red, whereas the signal of interest is shown in green.

Summarizing the discussion above, we have

$$|V_{Rx}| = M_{Tx,tag} M_{tag,Rx} \frac{4\pi^2 f^2 \epsilon |I_{Tx}| G_{Rx}}{Z_{tag}} \quad (1)$$

where G_{Rx} is the gain of the Rx chain including the filter and amplifiers.

We have $k_{Tx,tag} \propto r_{Tx,tag}^{-3}$ asymptotically [36], where $r_{Tx,tag}$ is the distance between Tx and tag. This leads to the $O(d^{-6})$ attenuation in signal energy with distance as described above.

3.2 Transmitter Design

InnerCompass provides a new transmitter design that helps enhance the strength of the measured signals that we receive. Traditional magnetic coils in near-field systems are generally connected in parallel to its tuning capacitor [30, 34, 48]. This can ensure that the coil draws minimum current from the power source at resonance, because parallel LC circuit have infinite impedance at resonance. This is important for modern "tight-design" devices like cell phones that have strict limit on power and heat dissipation. However, as we can see from Equation 3, the magnetic field strength is proportional to the current flowing through the coil. Therefore, to increase the operating range of InnerCompass, we need to increase the current that flows through the coil.

[1]The signal can also bounce multiple times among Tx, Rx and tag, but every hop brings an attenuation in the magnitude of k, therefore the multi-hop paths can be ignored.

We noticed that series LC circuits, in contrast to parallel ones, have zero impedance at resonance. This allow huge amount of current to flow with a low voltage source. Therefore, we designed our coils to have series LC circuit.

Moreover, traditional RF systems, both near-field and far field, ensure impedance matching on all input/output ports to 50Ω or 75Ω. This is to ensure that no signal is "reflected" at ports and Tx can transmit maximum **power** to the receiver. Even in traditional design of near field coils such as NFC, this rule of impedance matching is inherited and all prior works using inductive coupling communication devices use 50Ω amplifiers and matching circuit networks. However, we argue that this is not optimal for near field coupling where the signal strength depends solely on the magnetic field, and thus the **current** delivered to the Tx coil (not the *power* transmitted). Since a traditionally impedance-matched power amplifier has a high impedance of either 50Ω or 70Ω, it limits the current output (Ohm's law). Therefore, we used a low output impedance amplifier in InnerCompass to maximize the signal strength.

We will show in Section 4 and Section 5 that by just increasing the Tx current to a larger but still safe value, we will be able to increase the operating range of InnerCompass to a reasonable value that supports communication and localization in deep tissue. Moreover, the tag in human body is designed to be low power, and will not cause heat dissipation problem to human body. Finally, we will show in Section 5 that InnerCompass's operating radiation level is around 100dB lower than the safety limit and should cause no danger to human body.

3.3 Analytical Localization Model

InnerCompass designs an analytical model that maps the received signal of magnetic backscatter to the location of the implant. Unlike prior methods that use look up table or machine learning based localization models, InnerCompass's analytical model does not require an extensive set of data points for calibration. Rather InnerCompass's model relies primarily on the physics of the magnetic field to estimate an implant's location.

As discussed above, there are three main components in InnerCompass: the transmitter Tx, the receiver Rx, and the implanted device Tag. The coils of the transmitter, receiver and implant tag are placed in proximity of each other, and, as a result, generate a magnetic coupling with mutual inductance $M_{Tx,tag}$ and $M_{Rx,tag}$[2]. Furthermore, we observe that

- Our coils are made of thin wires, less than 0.5 mm in thickness. Therefore, the width and thickness of the Tx and Rx coils are significantly less than the radius of the coil, or the distance between the coil and the tag, so we can approximate the Tx and Rx coils with a simple current loop model.
- The size of the tag is required to be one or more order of magnitude smaller than the distance between the tag and Tx/Rx coils, so we can approximately assume that the tag is in a homogeneous magnetic field equal to the magnetic field at the center of the tag coil.

Given the second approximation, we can simplify the magnetic flux as $\Phi_{tag} = \mathbf{B} \cdot \mathbf{S}_{tag}$ where B is the magnetic field at any reference point on the coil and $\mathbf{S}_{tag}$ is the normal vector of the tag coil. We note that only $\mathbf{B}$ is associated with the tag's position.

Summarizing the discussion above, we can see that

$$M_{Tx,Tag} = \frac{\mathbf{B}_{Tx,Tag} \cdot \mathbf{S}_{tag}}{I} \tag{2}$$

where $B_{Tx,tag}$ is the magnetic field stimulated by the Tx coil current. We have similar conclusions for $M_{Rx,tag}$ too.

Finally, since we know the size of the coils, we just need to calculate $\mathbf{B}$ values for Equation 2. Our model estimates $\mathbf{B}$ by simply using the Biot – Savart law [9] described by the following equation:

$$\mathbf{B}(\mathbf{r}) = \frac{\mu_0}{4\pi} \int_C \frac{I d\boldsymbol{\ell} \times \mathbf{r}'}{|\mathbf{r}'|^3} \tag{3}$$

Where $\mathbf{r}'$ is the vector from the location of the current segment to the reference point $\mathbf{r}$. Because we simplify the Tx and Rx coils as current loops, we only need to take the integration in Equation 3 over a circle with given radius, which can easily be done using minimal compute power. From Equation 3 and Equation 2 we see that

$$M_{Tx,tag} = \frac{\mu_0}{4\pi} \int_C \frac{d\boldsymbol{\ell} \times \mathbf{r}'}{|\mathbf{r}'|^3} \cdot \mathbf{S}_{tag} \tag{4}$$

We define

$$B_{0n}(\mathbf{r}') = \frac{\mu_0}{4\pi} \int_C \frac{d\boldsymbol{\ell} \times \mathbf{r}'}{|\mathbf{r}'|^3} \cdot \hat{\mathbf{s}}$$

to be the the magnetic field caused by a unit of current ($I = 1$), projected to the normal vector of the tag coil surface ($\hat{\mathbf{s}}$), and we can see that

$$M_{Tx,tag} = B_{0n}\left(\mathbf{r}_{tag} - \mathbf{r}_{Tx}\right) S_{tag}$$

similarly,

$$M_{Rx,tag} = B_{0n}\left(\mathbf{r}_{tag} - \mathbf{r}_{Rx}\right) S_{tag}$$

We note that there is still one part of the model that needs calibration data from the real world: the constants for the "proportional to" relations in the model in Equation 1 and Equation 2. In principle, these could be obtained from the technical specifications of the components used, however, we can see that all the constants are multiplied together to get one "proportional" constant. Therefore, we can also just measure $|V|$ setting the tag at any given point, which would be sufficient to specify the constant. Note that, this needs to

[2]Note that mutual inductance is symmetric, $M_{tag,Rx} = M_{Rx,tag}$

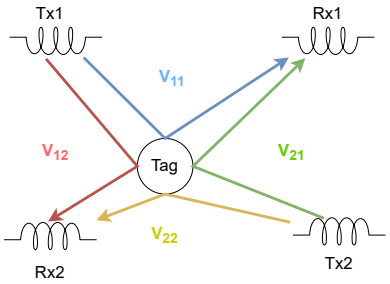

Figure 4: Illustration of the 4 RSSI values when there are 2 Tx and 2 Rx coils present

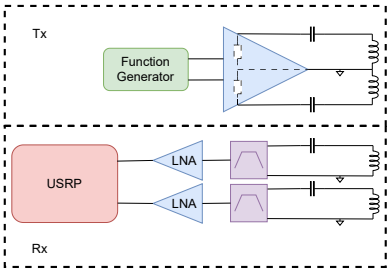

Figure 5: Composition of the reader's Tx and Rx chains. Each chain has 2 channels and 2 coils respectively

be only once and does not need to be repeated even when the tag is placed in a different environment or the reader coils change their relative position.

3.4 MIMO-Inspired Localization Strategy

Our model, discussed above, maps the signal strength of the received signal as a function of the relative location of the tag, with respect to the transmit and receive coils. To perform localization, we need to identify the location, (x, y), of the tag, given the measured signal strength values at the receiver. Since we need to identify these two variables, a single measurement is insufficient to identify the correct location of the tag.

Past work in magnetic tag readers use multiple Tx-Rx coils to generate multiple different measurements of the signal strength, and use these measurements to locate the tag. In these systems, each Tx coil communicates a designated Rx coil. Therefore, N Tx and N Rx coils generate N signal strength measurements. We argue that this is not the optimal strategy in precisely localizing the tag.

Instead, we borrow the idea of MIMO from RF communication to enable more measurement values. In MIMO, the receiver tries to estimate the wireless channel between each pair of Tx and Rx. In our design, the reader has multiple Tx coils and multiple Rx coils. We allow each of our Tx coils to choose a different frequency, Δf, thereby enabling frequency multiplexing. An outline of our MIMO measurement is displayed in Figure 4. Therefore, each Rx coil can receive the signal from *all* Tx coils simultaneously. Each Rx coil receives signal at N different frequencies, one for each Tx coil. This enables each receiver to distinguish between signal received from different transmitters, and measure the RSSI of all of them. By using this technique, InnerCompass can obtain N^2 measurements with just N Tx and Rx coils, compared to only N measurements in the prior work. More measurements enable more precise localization of the tag. We will demonstrate in Section 5 that by utilizing MIMO, it suffices to have 2 Txs and 2Rxs on the same axis to get a mm-precise 2D localization,

By utilizing the analytical model, we are able to build a mapping from location coordinates to signal strength values. We have 4 coils Tx1, Tx2, Rx1 and Rx2 at $(x_i, y_i), i \in Tx1, Tx2, Rx1, Rx2$. By applying Equation 1 we know that for any point (x, y), the received signal voltage is:

$$V_{ij}(x,y) = \frac{4\pi^2 f^2 |I_{Tx_i}| G_{Rx_j} S_{tag}^2}{Z_{tag}} \times B_{0n}\left(x - x_{Tx_i}, y - y_{Tx_i}, 0\right) B_{0n}\left(x - x_{Rx_j}, y - y_{Rx_j}, 0\right) \quad (5)$$

To go from signal strength measurements to underlying coordinates, we use a k-nearest neighbor (KNN) regression approach. We analytically compute the signal strength values over a mesh grid of step size 1mm on x and y. We compute the expected signal strength values on all the points in the grid according to Equation 5. We fit a KNN regression model using the (RSSIs, x, y) pairs. Once the model has been fit to the generated signal strength, given a set of signal strength value, InnerCompass can predict the location of the in-body tag.

4 IMPLEMENTATION

InnerCompass consists of two parts: an out-of-body reader and an in-body tag.

Reader Design: The components of the prototype reader are shown in Figure 5. The Tx chain consists of a 2-channel Teledyne T3AFG30 function generator, connected to a 2-channel Juntek DPA-2698 low-output-impedance power amplifier, which has an output impedance of no higher than 5Ω and supports up to $500mA$ current. The output port of the amplifier is connected to two Tx coils paired with the tuning capacitor for each channel. The two Tx channels operate at $f_1 = 5.95MHz, f_2 = 5.96MHz$ respectively to facilitate frequency multiplexing localization outlined in Section 3. We wrap 12 AWG magnetic wire around a machined piece of plastic to make the coils, which have a diameter of 39mm. The photo of the coil is displayed in Figure 6a. The Rx chain has 2

channels, and consists of 2 Rx coils of the same size as the Tx ones. The number of turns on Rx coils are different so that Rx resonates at the sideband frequency, not the carrier frequency. The Rx coils are connected to 2 impedance-matched muRata SFE5.74MC2 filters. The filter output is amplified by a ZFL-1000LN+ amplifier, and received by NI USRP-2904R SDR with an LFRX daughterboard.

Tag Design: We built a prototype of the tag shown in Figure 6a. The tag consists of a PA6512-AE coil and the receive chain. The receive chain operates using a coin battery, and includes a 10uF filtering capacitor, a DS1099U-BC+ clock signal generator, an ADG802 SPST analog switch, and a 180pF tuning capacitor. The circuit diagram is shown in Figure 6b. The clock generator generates a 262 kHz clock signal, which is mixed with the incoming signal to shift the input signal's frequency by $\Delta f = 262kHz$. The coil has a diameter of 8.38mm and thickness of 5.21mm, and can be fit into an edible capsule [21]. Our tag drains a current of $270\mu A$ and operates with a DC supply of 2.7-5.5V. Our tag would last more than 500 hours using a small coin battery.

4.1 Design Considerations and Variations

(i) Choosing the optimal design specs: We acknowledge that biomedical applications have divergent requirements on the range, power, and communication data rate. For example, [46] aims to detect EoE disease on the human neck, which can operate in a shorter range, while [12] uses in-body tags purely as beacons to estimate their location and doesn't require communication. Certain specs of components in InnerCompass can be altered to accommodate different requirements:

- **Operating frequency** As we can see from Equation 1, the signal strength increases with the frequency. However, when the frequency is higher, the near field approximation becomes worse, and the interaction of the signal with human body becomes more significant. Also, we have $V = 2\pi jfLI$ for the inductor. If the frequency becomes too high, there will be high voltage in the circuit which might be unsafe for humans.
- **Coil size** In general, a large coil's magnetic field is more "spread out" and a smaller coil's magnetic field is more "concentrated". When we make the coil larger, we get a longer range but the decay rate of the magnetic field becomes smaller, leading to a lower spatial resolution for localization. For example, [48] has a coil of $1.1m \times 0.9m$, and their signal attenuates by 10dB when the distance changes by 1.5m. In contrast, InnerCompass's signal strength decays by as much as 20dB when the distance changes by 9cm, yielding more than 30x spatial resolution.
- **Coil Q value** Q value determines a coil's bandwidth, as well as its impedance at resonance. Large Q value coils have smaller bandwidth, but resonate "stronger" at resonance and can generate stronger signals. One needs to balance between the operating range and communication bandwidth to choose the optimal coil.

In this paper, we used the setting that generates a range reasonably large for in-body localization (25cm) with high accuracy (mm level) and supports kbps level of communication that is suitable for a variety of applications.

(ii) Interference with Other Devices: In the real world, there may be other devices transmitting on the same frequency as InnerCompass, and it is important that InnerCompass neither causes interference to other transmission nor receives interference from other transmissions. Such interference is unlikely because InnerCompass operates in near field and has limited range. To test InnerCompass's far field effects, we simulated the radiation field of the Tx/Rx coil. It shows that on the sphere that is 3m away from the coil, the maximum electric field strength is $-96dBV/m$. On the other hand, the peak gain for the coil in InnerCompass is -110dB. In comparison, a typical half-wave dipole antenna has a gain of 2.15dB [4]. From the simulation results, we see that the ability of the coil to both emit and receive far field radiation is multiple orders of magnitude less than ordinary far field antennas. Therefore, it should not interfere with any external devices.

(iii) Safety to Human Body: As we will show in our experiments, InnerCompass causes human body absorption that is ∼100dB less than the FCC safety requirements. Also, the transmitter current is always less than the maximum output current of the amplifier which is 500mA. This is less than the current for commodity hardware such as a heated jacket, and is also several magnitudes less than [35].

On the other hand, the magnetic field generated by the Tx current loop at its center has the magnitude of $10^{-5}T$. This is comparable to the magnitude of the earth magnetic field[3]. We believe that such magnetic field should neither cause harm to human body nor interfere with any medical devices that has already been installed on the patient.

(iv) Scalability: It is straightforward to scale InnerCompass up to support multiple in-body devices, by adapting the NFC protocol which is multiplexed [48].

(v) Addressing Size Limits: Real-world medical applications have constraints on the size and power consumption, especially for in-body devices. InnerCompass's tag is currently implemented as a printed circuit board and as such is not optimized for size or power. However, we can see from

[3]However, InnerCompass is free from earth magnetic field interference because of the different frequency

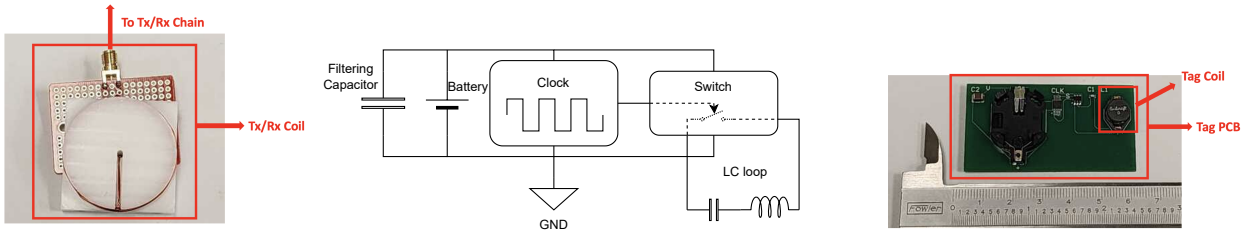

(a) InnerCompass's Transceiver Coils. **(b) InnerCompass circuit diagram.** **(c) InnerCompass tag PCB.**

Figure 6: InnerCompass Hardware Implementation (a-c): (a) Photo of InnerCompass's coils for the reader. (b) Circuit diagram for the tag in InnerCompass. (c) InnerCompass Tag PCB size measured with calipers.

Equation 2 that the size of the tag coil is the only part that affects the tag's ability to receive and reflect signal. A chip implementation of the rest of the transponder can reduce the overall size of the tag to the size of the coil. However, we leave such an implementation to future work.

Our tag size of 8.38mm in diameter can fit into most current applications. For example, in comparison, a "00" sized swallowable capsule has an outer diameter of 8.56mm. Commodity gastrointestinal endoscopy capsules have a diameter of up to 1.3cm [10]. Medical implants, on the other hand, can have a diameter of several cms [19].

Should it be required to reduce the coil size, note from Equation 1 that the signal $V_{Rx} \propto S_{tag}^2 \propto r^4$. The signal strength (RSSI) is proportional to V_{Rx}^2 [41, 42], and thus r^8. This means that when the diameter of the coil reduces by half, the signal strength will fall by 256× (24dB).

Such drop can be compensated by, e.g., reducing operating range. We know that asymptotically $B \propto d^{-3}$. So, from Equation 5, we know that $V_{Rx} \propto d^{-6}$. Therefore, we can see that with constant signal strength requirements (i.e. V_{Rx} being constant), $r^4 \times d^{-6}$ is constant. This implies that $d \propto r^{2/3}$, so the operating range decreases **slower** than the tag dimensions. For example, when the tag diameter is reduced by 2×, the operating range is reduced by 1.58×. The specific requirements of the size and operating range would depend on specific medical applications, and we leave such exploration to future work.

5 RESULTS

In this section, we evaluate InnerCompass's performance.

5.1 Testbed setup

To evaluate InnerCompass, we build a testbed as shown in Figure 7. We bought a glass aquarium of size 25cm×25cm×25cm with a perimeter of 100cm, similar to the size of a medium-sized adult waist. We set up a linear stage next to the aquarium to precisely adjust the position of the tag. We deployed the Tx and Rx coils of InnerCompass around the aquarium and placed pork ribs around our deployment along the sides of the aquarium to simulate the effect of human tissues, as shown in Figure 7b. We chose to use ribs as they are a complicated tissue that contains muscle, fat, blood, and bone, the majority types of tissues found inside human body. This is consistent with past work in this space [34, 35, 40]. We perform one-time calibration for the coils by placing the coil in the center of the aquarium in the free air environment. This calibration data is then used in all other environments, including in-body environment, and localization at new places.

5.2 Microbenchmarks

Human Body Absorption Simulation: We analyze InnerCompass's effect on the human body to determine whether or not it is safe for real-world deployment. We analyze this effect by simulating specific absorption rate (SAR) of InnerCompass at different parts of the human body using Ansys High Frequency Structure Simulator (HFSS) [5]. Fig. 8a plots the results of our simulation. We find that the maximum absorption rate in the body is -96 dB, while the FCC limit for SAR for wireless signal is 1.6W/kg, corresponding to 0.204dB. The SAR generated by InnerCompass is nearly 100dB less than the FCC safety limit, demonstrating that InnerCompass will not have a harmful impact on the human body.

Prediction Accuracy of the Analytical model: We aim to verify that our model's calculated RSSI values match real-world measurements in our setup. We measure the real-world magnetic field strength at a 10 by 10 grid in the center of the aquarium and plot the predicted and measured signal strength values in Figure 8b and Figure 8c respectively. Through visual inspection, the modeled and measured fields are nearly identical with only some slight differences due to noise in measurements for the real-world system.

We present aggregate statistics across different settings in Table 1. InnerCompass's modeled magnetic field in the setup uses only *a single point* of calibration data in free air to predict the magnetic field strength in both free air and pork ribs. The overall average prediction error is 1.73 dB. We can also see from the figure that when the position of the tag changes by 9cm, the RSSI changes by as much as

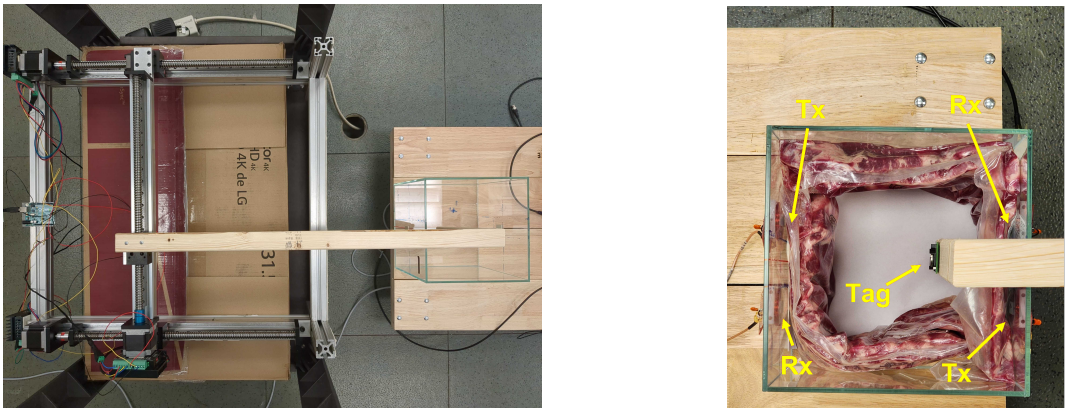

(a) Evaluation Platform (b) With Animal Tissue

Figure 7: Testbed: We use a 2D linear motion stage to enable precise motion of the tag inside an aquarium. We place pork ribs around the edges of the aquarium to simulate human tissue and cavities.

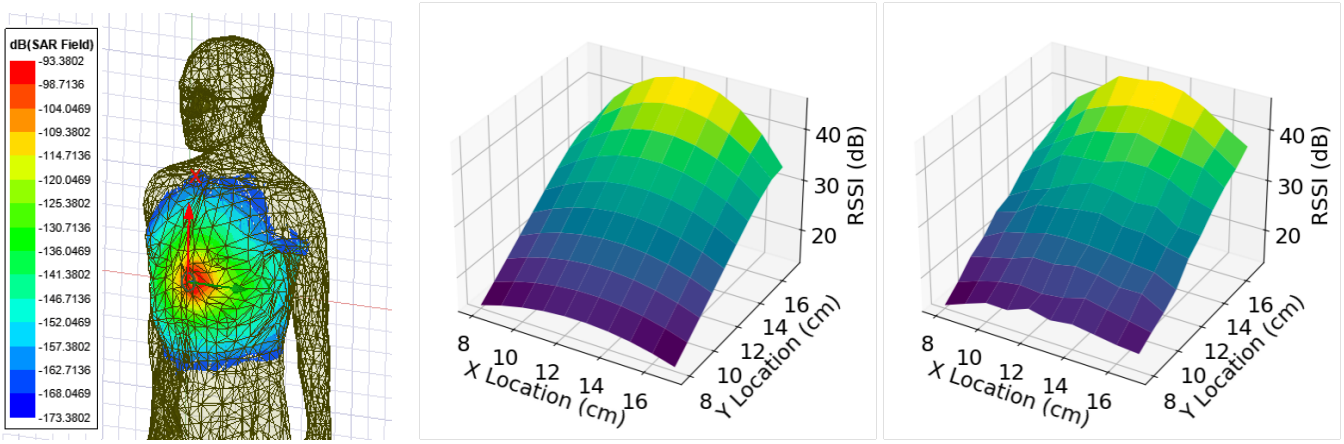

(a) SAR distribution over human body (b) Predicted RSSI values (c) Measured RSSI values

Figure 8: Microbenchmarks: (a) InnerCompass's tag has low specific absorption rate (SAR). (b) Our model's calculated RSSI values for V_{11}, (c) Measured RSSI values for V_{11} over the same points

approximately 25dB. The 1.73 dB predicting error would correspond to a 6.2mm displacement and is only 6.8% of the total dB variation. This microbenchmark validates our design choices and is encouraging for precise localization.

Animal Tissue's Impact on Signal: We measure the effect of animal tissue on received signal strength using pork tissue. We find that the signal strength is reduced by 1.68 dB on average by the presence of animal tissue. We also observe that the mean absolute difference between InnerCompass's prediction of signal strength and measured signal strength is 1.97 dB (more details in Table. 1). Overall, the animal tissue has a minimal impact on the signal strength as expected.

We believe that the minimal additional attenuation is due to a phenomenon called "damping effect", where when alternating magnetic field propagates inside conductive medium (animal tissue in this case), it stimulates eddy current that attenuates the magnetic field itself. The scale of this effect is positively correlated to the conductivity of the medium, and the proximity between the coils and the conductor.

Our evaluation environment, animal tissue, has a similar conductivity to human tissue. Also, as we will show, our evaluation includes cases where all the coils are less than 1cm from the animal tissue. InnerCompass being able to achieve high localization accuracy under such conditions indicates that the damping effect does not have a major adverse effect on its performance.

5.3 Localization: Accuracy

We evaluate InnerCompass's localization performance in two environments: a lab and an office. In each setting, we move the tag to hundred different locations within the aquarium on a 10 by 10 grid. The aquarium is surrounded by pork ribs. The ground truth location is output by the linear motion stage used to move the tag. We measure the error

Table 1: RSSI prediction error mean (std) for the analytic model vs real world (in dB). The average error is 1.73 dB across all experiments. Overall RSSI variation is approx. 25 dB across different tag positions.

Channel	Original (air)	Original (pork)	Unseen (pork)
V11	1.98 (1.58)	2.95 (2.37)	2.13 (1.56)
V12	1.13 (0.84)	2.24 (1.29)	1.06 (0.90)
V21	1.49 (1.22)	1.57 (1.43)	2.05 (1.52)
V22	0.55 (0.49)	1.15 (1.13)	2.49 (1.66)

between the ground truth location and estimated location and report it in Fig. 9. InnerCompass achieves a median error of 5.37 mm and 6.35 mm in the lab and office environment respectively. The variation in InnerCompass's localization performance at the median is less than 1mm, indicating that our system's performance does not degrade across different environments. Recall that InnerCompass does not include any location-specific calibration. This shows the accuracy of InnerCompass's localization strategy and demonstrates generalizability across environments. This is expected because near-field magnetic field does not experience multipath effects, unlike RF systems, and in general, are more generalizable across environments. Note that, for some evaluation locations in the grid, the tag coil is less than 1cm away from the film of the pork rib. This demonstrates that InnerCompass's tag works normally even when close to animal tissues. Therefore, we believe that InnerCompass should work robustly inside the human body.

5.4 Localization: Comparison to Baselines

We benchmark the localization performance of InnerCompass compared to other data-driven baselines. We compare InnerCompass to two commonly used in-body localization baselines: 1) a lookup table [31, 35, 47] and 2) a neural-network-based model using a multi-layer perceptron [26, 33]. Since the baselines rely on data-driven approaches, we train these baselines with a random subset of calibration data collected across our grid in the same environment. InnerCompass's analytical model, however, is calibrated with only a single point of data at *manufacture time*, i.e., no per experiment calibration. In Fig. 10a, we plot the median and 1 standard deviation error bars of the resulting localization errors in different calibration experiments. The median localization error of InnerCompass is 5.37mm. We observe that all 3 models converge to around this same localization error; but with multiple training points. InnerCompass's analytical approach compares favorably to state-of-the-art baselines. Since it does not require data-driven training, it is easier and faster to modify InnerCompass's analytical model to suit different body shapes or apply for different deployment

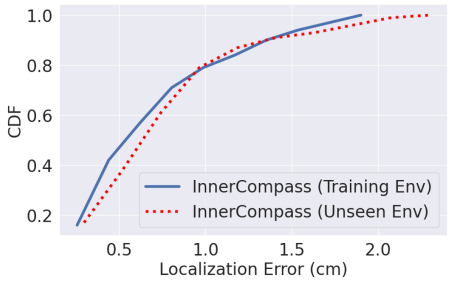

Figure 9: Localization Accuracy: InnerCompass can achieve a median localization accuracy of 5.37 mm and 6.35 mm in lab and office environments respectively.

behaviors. This is especially useful in the context of wearable devices such as belts where the relative position of the reader coils may move over time or need to be adjusted based on patient movement or size.

5.5 Localization: Generalizability

We already evaluated InnerCompass's ability to generalize to different environments. Next, we evaluate InnerCompass's ability to generalize to different horizontal planes for the implanted tag motion. In this experiment, we shifted the implant tag's motion plane to be 31.6mm lower relative to the original evaluation plane. We collected the RSSI values over our grid with this new position. Since InnerCompass can simply create a new magnetic field distribution, it does not need to collect any new data at this plane. Instead, we modify the z value in Equation 5 to be $-31.6mm$ to generate the new analytic RSSI values. For the baseline models, we use the original measurement data from the non-shifted tag experiments, i.e., we do not collect any new data for them. Both baselines use 100 points to train the models. Fig. 10b plots the CDF of localization error for all models across this experiment. The median localization error for InnerCompass is 4.3mm while the median localization errors for the lookup table and perceptron baselines are 7.5 mm and 5.1 mm respectively. We observe that InnerCompass significantly outperforms the baseline models in terms of generalizing to the new tag position with just a single calibration point. Even with 100 points of calibration data, the baselines still perform worse in the generalization setting and are likely over-fitting to the position of the tag in the calibration setting. In a real-world setting, the implant tag is likely to move around or travel within the human body.

5.6 Localization: MIMO Benefits

We next examine the effect of our MIMO localization strategy. We modify InnerCompass's model to only measure 2 RSSI values on the 2 Tx, Rx pairs, rather than using the current

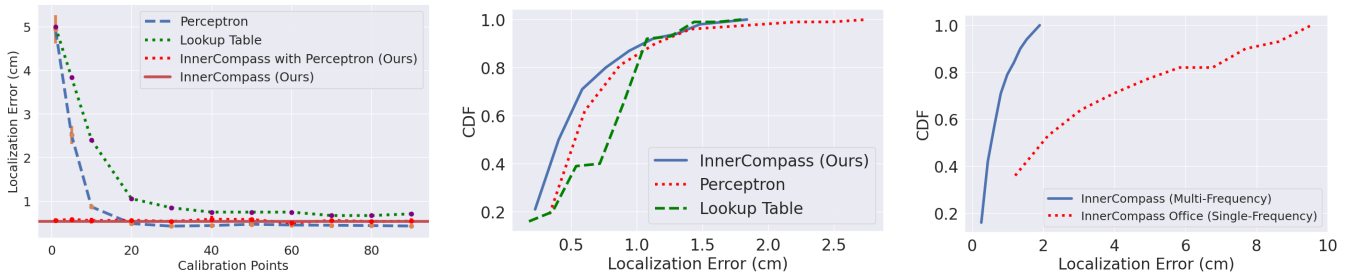

(a) Comparison to Baselines (b) Generalizability (c) MIMO Benefits

Figure 10: InnerCompass Localization: (a) State-of-the-art baselines have higher errors and/or require training on multiple data points. (b) InnerCompass can generalize without needing re-calibration. (c) InnerCompass's MIMO approach significantly aids localization.

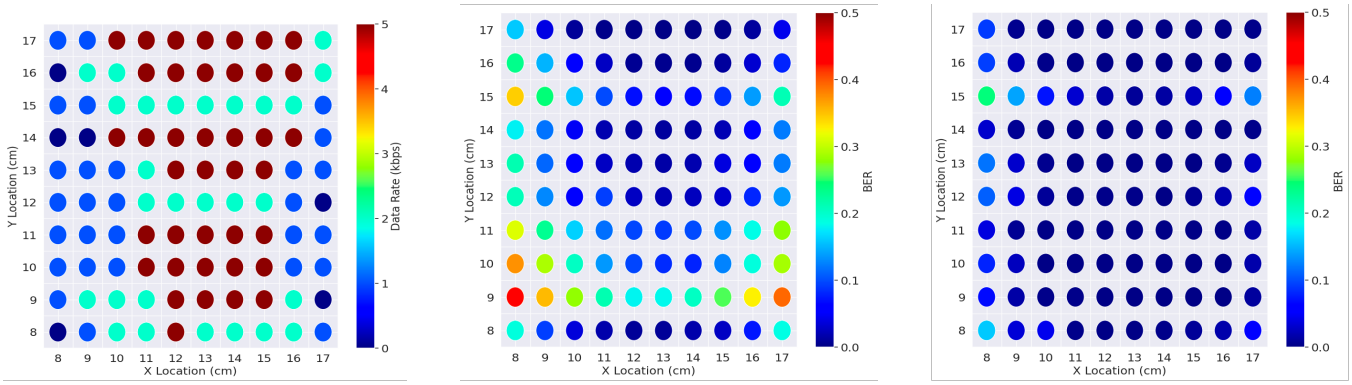

(a) InnerCompass Data Rate. (b) Traditional Transmitter Design. (c) InnerCompass's Transmitter Design.

Figure 11: Communication (a-c): (a) Maximum bitrate that InnerCompass can support with a bit error rate less than 10^{-3} (b) BER for 5kbps communication for the "traditional" transmitter design with 50Ω impedance and parallel LC circuit (c) BER for 5kbps communication using InnerCompass's low impedance series LC transmitter design

setup that allows all receivers to distinguish frequency signal from all transmitters. Fig. 10c reports the CDF of localization error across the grid with both experimental setups. The median localization error without our MIMO localization technique is 19.7 mm and the median location error with our technique is 5.3 mm. The performance of InnerCompass without leveraging the multiple coils on different frequencies is nearly 4 × worse. Naturally, more measurements yield a more precise location of the tag, and collecting these measurements through frequency multiplexing ensures that InnerCompass will be able to achieve mm-level localization accuracy without having to scale to an unreasonable amount of tx-rx pairs.

5.7 Communication: Datarate

Lastly, we evaluate InnerCompass's data communication system. To enable InnerCompass's tag to send data, we added a data path to the PCB and used a functional generator to transfer the bits. We set up 1 Tx and 1 Rx coil on the center of each side of the aquarium. InnerCompass's tag modulates data using a simple on-off-keying scheme. InnerCompass's tag transmits data at four different data rates: 500 bps, 1kbps, 2kbps, and 5kbps. Fig. 11a plots the maximum data rate at each spot in our grid where InnerCompass can achieve a bit error rate of less than 0.001. Note that the motion of the tag is limited due to the presence of meat in the aquarium (one corner of the aquarium is (0,0)). We find that InnerCompass achieves higher data rates at locations where x position is between 9 cm and 15 cm. This phenomenon is likely due to that the points on the edge are far from both Tx and Rx, and have low SNR according to Equation 1. To fix this problem, one can simply use multiple sets of coils to cover different parts of the field of view. InnerCompass is capable of easily transmitting localization data and even low-resolution images from within various parts of the body. The high data rates that InnerCompass is capable of achieving can be credited to the novel transmitter design used in the system. By providing increased current and signal strength, our novel transmitter design empowers InnerCompass to achieve high SNRs at long ranges.

5.8 Communication: Low Impedance Transmitter Design

To validate our design of the custom low-impedance amplifier and series LC coil, we switched the transmitter with a parallel LC design having the same specs as the original transmitter, removed the power amplifier from the Tx chain, and changed the output amplitude of the function generator to 2× its original value to emulate a 50Ω RF amplified (the low impedance PA has a gain of 2× and the function generator has an output impedance of 50Ω). We then repeated the communication experiment, setting the data transmission rate to 5kbps. We compare the BER at different grid points in Figure 11c and Figure 11b. We can see that the BER rate increased by 9.4× on average. This validates that our antenna design increases signal strength and communication quality.

5.9 Robustness to Magnetic Interference

We evaluate InnerCompass's robustness to magnetic interference. To conduct this experiment, we generate magnetic interference through the motor from the linear-stage in our deployment testbed. When switched on, we observe that the motor from the stage generates a magnetic field that creates interference for InnerCompass. In our setup, the motor is deployed approximately 15cm away from the InnerCompass implant tag. Fig. 12 plots the spectrum measured from the Rx antennas in our deployment with and without magnetic inference from the motor. We observe that magnetic interference does have some effect on the spectrum and raises the noise floor. This can slightly reduce the SNR in communication settings and require transmission at a lower data rate. However, we find that as long as the source of magnetic interference is far enough (around 15cm in our setup), InnerCompass's performance does not degrade. This is evidenced in spectrum measurement from Fig. 12 as we see the frequency peaks in 5.688MHz and 5.698MHz corresponding to the two expected side-band frequencies for the 2 Tx channels in our deployment. Robustness against magnetic interference is a necessity for in-body communication systems deployed as part of wearable devices. Outside of a hospital or controlled medical setting, there are many potential sources of interference that could be detrimental to in-body systems for at-home health monitoring applications. InnerCompass's robustness against these sources of interference come from the novel antenna design, which improves both the generated current and magnetic field strength. As a result, the overall signal strength received from InnerCompass's implant tag is high enough to be above the increased noise floor caused by magnetic interference.

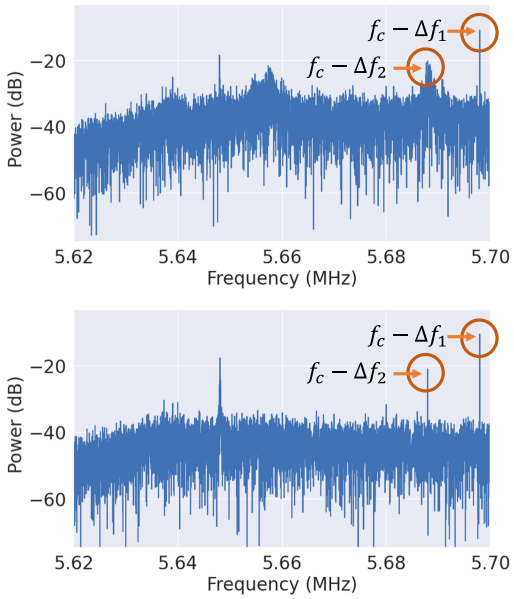

Figure 12: Spectrum of InnerCompass with magnetic interference (above) and without magnetic interference (below). Reflected signal at 5.688MHz and 5.698MHz can be detected in both experiments.

6 RELATED WORK

RF-Based In-Body Systems: There has been a large body of work that has used wireless technology to communicate and localize in-body implantable devices [3, 8, 28, 38, 40, 49]. The majority of these efforts have relied on RF signals which suffer from a variety of phenomena when passing through the human body. There have been many attempts to solve these challenges in prior work, some of which include lack of wireless channel feedback [23], variable tissue characteristics [2], and power transfer [16]. Additionally, many of these RF-based communication systems suffer from rapid attenuation when passing through the body [7, 20, 32]. They operate at very limited distance ranges and typically only support devices implanted at the surface of the human body rather than deep tissue implants. For example, [25]'s glucose sensor needs to be inserted under the skin and cannot communicate from deep tissue. On the other hand, InnerCompass provides a much simpler solution with a magnetic signal-based approach. Unlike RF-based signals, the magnetic signals used in InnerCompass are completely unaffected by the human body and do not suffer from problematic phenomena such as attenuation and the multi-path effect. As a result, there are fewer challenges for in-body sensing using magnetic signals.

Magnetic In-Body Systems: Prior research efforts have also designed magnetic systems for in-body implants. Some of these systems are purely designed for communication [45] and do not provide any localization capabilities. However,

Table 2: Comparison of InnerCompass against prior work on magnetic in-body systems in terms of features.

Prior Work	Feature					
	Localization Error (mm)	Data Rate (kbps)	Max Tag Power (mW)	Range* (cm)	Is Small?	Is Safe?
NFC+ [48]	N/A	6.7	0†	300	✗	✗
NFCapsule [46]	N/A	N/A	0†	5.5	✓	✓
Rustom & Sideris [34]	1	N/A	6	20	✗	✓
Ray et al. [30]	10	N/A	0†	4	✓	✓
Yu et al. [44]	N/A	1	0†	1.5	✓	✓
Sharma et al. [35]	5	N/A	24	20	✗	✗
Ours	5	5	0.73	17.5	✓	✓

* *Measured by the maximum distance to the closest Tx/Rx antenna.*
† *Passive tag.*

for those systems that provide localization [31, 35, 47] capabilities lie two fundamental flaws: 1) calibration and 2) generalizability. Prior systems build a magnetic localization model by either using lookup tables [31, 35, 47] or using machine learning [34] based techniques. These types of models require a significant amount of measured data to properly calibrate (for example, [34] collected measurements on over 68921 grid points). Moreover, these models do not generalize well to different environments and body types, and they need to be re-calibrated every time the positions of the antennas need to be adjusted. InnerCompass, on the other hand, designs an analytical and *calibration-free* model for localization based on the physics of the magnetic field generated by the antennas. Our approach avoids cumbersome data collection required for calibration and generalizes well to a variety of different environments. Moreover, the prior works have other design limits that prevent them from being deployed to something like a smart wearable. We summarize the limits of the prior work in Table 2

Near Field Communication (NFC): Similar to our work, NFC also based on the principle of inductive magnetic coupling. Rather than localization, NFC uses magnetic coupling of coils in proximity of each other to transmit data. A unique characteristic of NFC communication is that its range is limited to few millimeters, making it an ideal technology for secure transactions such as contact less payments [11], identity control [29], etc.

However, in other contexts, NFC's limited range has been viewed as a drawback. To enable longer range applications such as RFID system through NFC, prior work has managed to increase the range of NFC to by engineering a modified magnetic field reader [48]. However, unlike InnerCompass this system uses a mag-repeater that would make the RSSI-distance relation non-monotonic, which could complicated localization efforts. Additionally, the tag coil size is of this system is too large to place inside the human body.

7 CONCLUDING DISCUSSION

We present InnerCompass, a magnetism-based communication and localization system for in-body devices. Our system operates in deep-tissue, achieves mm-level localization accuracy, provides kbps communication with low BER, and does not require fingerprinting. Our current design has two limitations that we hope to address in future work:

- **Rotation:** Our current design needs to know the orientation of the tag. Since magnetic coupling is dependent on alignment, in future work, we plan to model the rotation as another unknown variable that we estimate using magnetic field measurements. Estimating more unknown variables requires more measurements from additional coils. We leave this exploration to future work.
- **Flexible Designs:** We envision InnerCompass to be a smart wearable in the future, e.g., a smart belt or vest, that can be a platform to connect to all in-body devices. The belt design however requires us to accommodate variable reader coil locations. Our current design needs to know the position of reader coils. In future work, we plan to automatically estimate the position of the reader coils using cross-coil coupling measurements. Note that, fingerprinting-based systems cannot solve this use case because they need to collect new training data every time the locations of the reader coils change.

Acknowledgments — We thank the reviewers and our anonymous shepherd for their insightful comments and suggestions on improving this paper. We are grateful to Maleeha Masood, Ishani Janveja, Zikun Liu, and Om Chabra for their feedback on initial drafts. We thank Abigail Barrett for logistical support to this project. We thank Mengze Sha, Rakibul Islam and Hyunjoo Seo for their feedback on circuit design.

REFERENCES

[1] Qammer H Abbasi, Masood Ur Rehman, Khalid Qaraqe, and Akram Alomainy. 2016. *Advances in body-centric wireless communication: Applications and state-of-the-art.* Institution of Engineering and Technology.

[2] Mohamed R Abdelhamid, Ruicong Chen, Joonhyuk Cho, Anantha P Chandrakasan, and Fadel Adib. 2020. Self-reconfigurable microimplants for cross-tissue wireless and batteryless connectivity. In *MobiCom'20: Proceedings of the 26th Annual International Conference on Mobile Computing and Networking*.

[3] Mohamed R Abdelhamid, U Ha, Utsav Banerjee, Fadel Adib, and A Chandrakasan. 2022. Wireless, Batteryless, and Secure Implantable System-on-a-Chip for 1.37 mmHg Strain Sensing with Bandwidth Reconfigurability for Cross-Tissue Adaptation. In *2022 IEEE Custom Integrated Circuits Conference (CICC)*. IEEE, 1–2.

[4] Constantine A. Balanis. [n. d.]. *Antenna Theory: Analysis and Design*. Wiley-Interscience.

[5] Zoltan Cendes. [n. d.]. The development of HFSS. In *2016 USNC-URSI Radio Science Meeting* (Fajardo, PR, USA, 2016-06). IEEE, 39–40. https://doi.org/10.1109/USNC-URSI.2016.7588501

[6] Mayo Clinic. [n. d.]. Capsule endoscopy. https://www.mayoclinic.org/tests-procedures/capsule-endoscopy/about/pac-20393366.

[7] Andrew DeHennis, Stefan Getzlaff, David Grice, and Marko Mailand. 2015. An NFC-enabled CMOS IC for a wireless fully implantable glucose sensor. *IEEE journal of biomedical and health informatics* 20, 1 (2015), 18–28.

[8] Ilka Dove. 2014. *Analysis of radio propagation inside the human body for in-body localization purposes.* Master's thesis. University of Twente.

[9] Richard Fitzpatrick. 2006. Classical electromagnetism. Vol. 149. Chapter 7.

[10] UCSF Health. 2019. Capsule endoscopy. https://www.ucsfhealth.org/medical-tests/capsule-endoscopy.

[11] EL Hillali, Jaouad Boutahar, and Souhail EL. 2017. NFC Technology for Contactless Payment Echosystems. *International Journal of Advanced Computer Science and Applications* 8 (01 2017). https://doi.org/10.14569/IJACSA.2017.080548

[12] Henkjan J. Huisman, Jurgen J. Fütterer, Emile N. J. T. van Lin, Arjan Welmers, Tom W. J. Scheenen, Jorn A. van Dalen, Andries G. Visser, J. A. Witjes, and Jelle O. Barentsz. [n. d.]. Prostate Cancer: Precision of Integrating Functional MR Imaging with Radiation Therapy Treatment by Using Fiducial Gold Markers. 236, 1 ([n. d.]), 311–317. https://doi.org/10.1148/radiol.2361040560

[13] Veronica Iacovacci, Izadyar Tamadon, Emanuele Federico Kauffmann, Stefano Pane, Virginia Simoni, Leonardo Marziale, Michele Aragona, Luigi Cobuccio, Massimo Chiarugi, Paolo Dario, Stefano Del Prato, Leonardo Ricotti, Fabio Vistoli, and Arianna Menciassi. [n. d.]. A fully implantable device for intraperitoneal drug delivery refilled by ingestible capsules. 6, 57 ([n. d.]), eabh3328. https://doi.org/10.1126/scirobotics.abh3328

[14] Gavriel Iddan, Gavriel Meron, Arkady Glukhovsky, and Paul Swain. 2000. Wireless capsule endoscopy. *Nature* 405, 6785 (2000), 417–417.

[15] Abhinanda Kar, Nadim Ahamad, Mahima Dewani, Lisha Awasthi, Runali Patil, and Rinti Banerjee. [n. d.]. Wearable and implantable devices for drug delivery: Applications and challenges. 283 ([n. d.]), 121435. https://doi.org/10.1016/j.biomaterials.2022.121435

[16] Sadeque Reza Khan, Sumanth Kumar Pavuluri, Gerard Cummins, and Marc PY Desmulliez. 2020. Wireless power transfer techniques for implantable medical devices: A review. *Sensors* 20, 12 (2020), 3487.

[17] Manikanta Kotaru, Kiran Joshi, Dinesh Bharadia, and Sachin Katti. [n. d.]. SpotFi: Decimeter Level Localization Using WiFi. In *Proceedings of the 2015 ACM Conference on Special Interest Group on Data Communication* (London United Kingdom, 2015-08-17). ACM, 269–282. https://doi.org/10.1145/2785956.2787487

[18] Hideo D Kubo and Bruce C Hill. [n. d.]. Respiration gated radiotherapy treatment: a technical study. 41, 1 ([n. d.]), 83–91. https://doi.org/10.1088/0031-9155/41/1/007

[19] Kyeongha Kwon, Jong Uk Kim, Sang Min Won, Jianzhong Zhao, Raudel Avila, Heling Wang, Keum San Chun, Hokyung Jang, Kun Hyuck Lee, Jae-Hwan Kim, et al. 2023. A battery-less wireless implant for the continuous monitoring of vascular pressure, flow rate and temperature. *Nature Biomedical Engineering* (2023), 1–14.

[20] Antonio Lazaro, Marti Boada, Ramon Villarino, and David Girbau. 2019. Study on the reading of energy-harvested implanted NFC tags using mobile phones. *IEEE Access* 8 (2019), 2200–2221.

[21] Dong-Hwan Lee, Joong-Hyun Song, DoHyeon Yu, Su-Jin An, Hee-Chun Lee, Young Joo Kim, Donghyun Han, and Dong-In Jung. 2019. A study on the difference of gastrointestinal transit time with minimized capsule endoscope in dogs. *Journal of Biomedical Translational Research* 20, 3 (2019), 65–70. https://doi.org/10.12729/jbtr.2019.20.3.065

[22] Ho-Yu Lin, Masaharu Takahashi, Kazuyuki Saito, and Koichi Ito. 2012. Performance of implantable folded dipole antenna for in-body wireless communication. *IEEE Transactions on Antennas and Propagation* 61, 3 (2012), 1363–1370.

[23] Yunfei Ma, Zhihong Luo, Christoph Steiger, Giovanni Traverso, and Fadel Adib. 2018. Enabling deep-tissue networking for miniature medical devices. In *Proceedings of the 2018 Conference of the ACM Special Interest Group on Data Communication*. 417–431.

[24] Matteo Maspero, Peter R. Seevinck, Nicole J. W. Willems, Gonda G. Sikkes, Geja J. de Kogel, Hans C. J. de Boer, Jochem R. N. van der Voort van Zyp, and Cornelis A. T. van den Berg. [n. d.]. Evaluation of gold fiducial marker manual localisation for magnetic resonance-only prostate radiotherapy. 13, 1 ([n. d.]), 105. https://doi.org/10.1186/s13014-018-1029-7

[25] NIDDK. [n. d.]. *Continuous Glucose Monitoring*. https://www.niddk.nih.gov/health-information/diabetes/overview/managing-diabetes/continuous-glucose-monitoring

[26] S.K. Pal and S. Mitra. [n. d.]. Multilayer perceptron, fuzzy sets, and classification. 3, 5 ([n. d.]), 683–697. https://doi.org/10.1109/72.159058

[27] Duc Pham and Syed Mahfuzul Aziz. [n. d.]. A Real-Time Localization System for an Endoscopic Capsule Using Magnetic Sensors. 14, 11 ([n. d.]), 20910–20929. https://doi.org/10.3390/s141120910

[28] Mohammad Pourhomayoun, Mark Fowler, and Zhanpeng Jin. 2012. A novel method for medical implant in-body localization. In *2012 Annual International Conference of the IEEE Engineering in Medicine and Biology Society*. IEEE, 5757–5760.

[29] Emanuele Raso, Giulio Maria Bianco, Lorenzo Bracciale, Gaetano Marrocco, Cecilia Occhiuzzi, and Pierpaolo Loreti. 2022. Privacy-Aware Architectures for NFC and RFID Sensors in Healthcare Applications. *Sensors* 22, 24 (2022). https://doi.org/10.3390/s22249692

[30] Arkaprova Ray, Iman Habibagahi, and Aydin Babakhani. [n. d.]. Fully Wireless and Batteryless Localization and Physiological Motion Detection System for Point-of-care Biomedical Applications. In *2022 IEEE Biomedical Circuits and Systems Conference (BioCAS)* (Taipei, Taiwan, 2022-10-13). IEEE, 26–30. https://doi.org/10.1109/BioCAS54905.2022.9948647

[31] Arkaprova Ray, Iman Habibagahi, and Aydin Babakhani. 2022. Fully Wireless and Batteryless Localization and Physiological Motion Detection System for Point-of-care Biomedical Applications. In *2022 IEEE Biomedical Circuits and Systems Conference (BioCAS)*. 26–30. https://doi.org/10.1109/BioCAS54905.2022.9948647

[32] Bruno MG Rosa, Salzitsa Anastasova, and Guang Z Yang. 2021. NFC-powered implantable device for on-body parameters monitoring with secure data exchange link to a medical blockchain type of network.

IEEE Transactions on Cybernetics (2021).

[33] F. Rosenblatt. [n. d.]. The perceptron: A probabilistic model for information storage and organization in the brain. 65, 6 ([n. d.]), 386–408. https://doi.org/10.1037/h0042519

[34] Michella Rustom and Constantine Sideris. [n. d.]. Wireless Frequency-Division Multiplexed 3D Magnetic Localization for Low Power Sub-mm Precision Capsule Endoscopy. In *2022 IEEE Custom Integrated Circuits Conference (CICC)* (Newport Beach, CA, USA, 2022-04). IEEE, 01–02. https://doi.org/10.1109/CICC53496.2022.9772802

[35] Saransh Sharma, Khalil Ramadi, Nikhil Poole, Shriya Srinivasan, Keiko Ishida, Johannes Kuosmanen, Josh Jenkins, Fatemeh Aghlmand, Margaret Swift, Mikhail Shapiro, Giovanni Traverso, and Azita Emami. 2023. Location-aware ingestible microdevices for wireless monitoring of gastrointestinal dynamics. *Nature Electronics* (02 2023), 1–15. https://doi.org/10.1038/s41928-023-00916-0

[36] James C Simpson, John E Lane, Christopher D Immer, and Robert C Youngquist. 2001. *Simple analytic expressions for the magnetic field of a circular current loop.* Technical Report.

[37] Shriya S. Srinivasan, Amro Alshareef, Alexandria V. Hwang, Ziliang Kang, Johannes Kuosmanen, Keiko Ishida, Joshua Jenkins, Sabrina Liu, Wiam Abdalla Mohammed Madani, Jochen Lennerz, Alison Hayward, Josh Morimoto, Nina Fitzgerald, Robert Langer, and Giovanni Traverso. [n. d.]. RoboCap: Robotic mucus-clearing capsule for enhanced drug delivery in the gastrointestinal tract. 7, 70 ([n. d.]), eabp9066. https://doi.org/10.1126/scirobotics.abp9066

[38] Timo Sztyler and Heiner Stuckenschmidt. 2016. On-body localization of wearable devices: An investigation of position-aware activity recognition. In *2016 IEEE International Conference on Pervasive Computing and Communications (PerCom)*. IEEE, 1–9.

[39] Mehmet Efe Tiryaki, Fatih Dogangun, Cem Balda Dayan, Paul Wrede, and Metin Sitti. [n. d.]. MRI-powered Magnetic Miniature Capsule Robot with HIFU-controlled On-demand Drug Delivery. ([n. d.]). https://doi.org/10.48550/ARXIV.2301.07197 Publisher: arXiv Version Number: 1.

[40] Deepak Vasisht, Guo Zhang, Omid Abari, Hsiao-Ming Lu, Jacob Flanz, and Dina Katabi. 2018. In-body backscatter communication and localization. In *Proceedings of the 2018 Conference of the ACM Special Interest Group on Data Communication*. 132–146.

[41] Wikipedia. 2023. Electric power — Wikipedia, The Free Encyclopedia. http://en.wikipedia.org/w/index.php?title=Electric%20power&oldid=1169959330. [Online; accessed 14-August-2023].

[42] Wikipedia. 2023. Received signal strength indicator — Wikipedia, The Free Encyclopedia. http://en.wikipedia.org/w/index.php?title=Received%20signal%20strength%20indicator&oldid=1147491776. [Online; accessed 14-August-2023].

[43] Jie Xiong and Kyle Jamieson. [n. d.]. ArrayTrack: a fine-grained indoor location system. In *Proceedings of the 10th USENIX conference on Networked Systems Design and Implementation* (USA, 2013-04-02) *(nsdi'13)*. USENIX Association, 71–84.

[44] Zhanghao Yu, Fatima T. Alrashdan, Wei Wang, Matthew Parker, Xinyu Chen, Frank Y. Chen, Joshua Woods, Zhiyu Chen, Jacob T. Robinson, and Kaiyuan Yang. [n. d.]. Magnetoelectric backscatter communication for millimeter-sized wireless biomedical implants. In *Proceedings of the 28th Annual International Conference on Mobile Computing And Networking* (Sydney NSW Australia, 2022-10-14). ACM, 432–445. https://doi.org/10.1145/3495243.3560541

[45] Zhanghao Yu, Fatima T. Alrashdan, Wei Wang, Matthew Parker, Xinyu Chen, Frank Y. Chen, Joshua Woods, Zhiyu Chen, Jacob T. Robinson, and Kaiyuan Yang. 2022. Magnetoelectric Backscatter Communication for Millimeter-Sized Wireless Biomedical Implants. In *Proceedings of the 28th Annual International Conference on Mobile Computing And Networking* (Sydney, NSW, Australia) *(MobiCom '22)*. Association for Computing Machinery, New York, NY, USA, 432–445. https://doi.org/10.1145/3495243.3560541

[46] Junbo Zhang, Gaurav Balakrishnan, Sruti Srinidhi, Arnav Bhat, Swarun Kumar, and Christopher Bettinger. [n. d.]. NFCapsule: An Ingestible Sensor Pill for Eosinophilic Esophagitis Detection Based on near-Field Coupling. In *Proceedings of the Twentieth ACM Conference on Embedded Networked Sensor Systems* (Boston Massachusetts, 2022-11-06). ACM, 75–90. https://doi.org/10.1145/3560905.3568523

[47] Junbo Zhang, Gaurav Balakrishnan, Sruti Srinidhi, Arnav Bhat, Swarun Kumar, and Christopher Bettinger. 2023. NFCapsule: An Ingestible Sensor Pill for Eosinophilic Esophagitis Detection Based on near-Field Coupling. In *Proceedings of the 20th ACM Conference on Embedded Networked Sensor Systems* (Boston, Massachusetts) *(SenSys '22)*. Association for Computing Machinery, New York, NY, USA, 75–90. https://doi.org/10.1145/3560905.3568523

[48] Renjie Zhao, Purui Wang, Yunfei Ma, Pengyu Zhang, Hongqiang Harry Liu, Xianshang Lin, Xinyu Zhang, Chenren Xu, and Ming Zhang. 2020. Nfc+ breaking nfc networking limits through resonance engineering. In *Proceedings of the Annual conference of the ACM Special Interest Group on Data Communication on the applications, technologies, architectures, and protocols for computer communication*. 694–707.

[49] Guanglou Zheng, Rajan Shankaran, Mehmet A Orgun, Li Qiao, and Kashif Saleem. 2016. Ideas and challenges for securing wireless implantable medical devices: A review. *IEEE Sensors Journal* 17, 3 (2016), 562–576.